Neurobiology of Disease

Effects in Neocortical Neurons of Mutations of the $Na_v1.2$ Na^+ Channel causing Benign Familial Neonatal-Infantile Seizures

Paolo Scalmani,[1] Raffaella Rusconi,[1] Elena Armatura,[1] Federico Zara,[2] Giuliano Avanzini,[1] Silvana Franceschetti,[1] and Massimo Mantegazza[1]

[1]Department of Neurophysiopathology, Istituto Neurologico C. Besta, 20133 Milan, Italy, and [2]Laboratory of Neurogenetics, Unit of Muscular and Neurodegenerative Disease, Istituto G. Gaslini, University of Genova, 16147 Genova, Italy

Mutations of voltage-gated Na^+ channels are the most common cause of familial epilepsy. Benign familial neonatal-infantile seizures (BFNIS) is an epileptic trait of the early infancy, and it is the only well characterized epileptic syndrome caused exclusively by mutations of $Na_v1.2$ Na^+ channels, but no functional studies of BFNIS mutations have been done. The comparative study of the functional effects and the elucidation of the pathogenic mechanisms of epileptogenic mutations is essential for designing targeted and effective therapies. However, the functional properties of Na^+ channels and the effects of their mutations are very sensitive to the cell background and thus to the expression system used. We investigated the functional effects of four of the six BFNIS mutations identified (L1330F, L1563V, R223Q, and R1319Q) using as expression system transfected pyramidal and bipolar neocortical neurons in short primary cultures, which have small endogenous Na^+ current and thus permit the selective study of transfected channels. The mutation L1330F caused a positive shift of the inactivation curve, and the mutation L1563V caused a negative shift of the activation curve, effects that are consistent with neuronal hyperexcitability. The mutations R223Q and R1319Q mainly caused positive shifts of both activation and inactivation curves, effects that cannot be directly associated with a specific modification of excitability. Using physiological stimuli in voltage-clamp experiments, we showed that these mutations increase both subthreshold and action Na^+ currents, consistently with hyperexcitability. Thus, the pathogenic mechanism of BFNIS mutations is neuronal hyperexcitability caused by increased Na^+ current.

Key words: **sodium channel; epilepsy; cortex; excitability; current; neonatal; seizures**

Introduction

Mutations in the genes encoding neuronal voltage-gated Na^+ channels are the most common known genetic cause of familial epilepsy, causing severe myoclonic epilepsy of infancy (SMEI), generalized epilepsy with febrile seizures plus (GEFS+), simple febrile seizures, benign familial infantile seizures (BFIS), and benign familial neonatal-infantile seizures (BFNIS) (Avanzini and Franceschetti, 2003; Noebels, 2003; George, 2005; Mantegazza et al., 2005a; Meisler and Kearney, 2005; Striano et al., 2006). Voltage-gated Na^+ channels are heteromeric complexes formed by a principal pore-forming and voltage-sensing α subunit and by accessory β subunits. The primary sequence of the α subunit contains four homologous domains (DI–DIV), each containing six transmembrane segments (S1–S6); the β subunits contain a single transmembrane segment. Nine α subunits ($Na_v1.1$–$Na_v1.9$) and four β subunits ($\beta1$–$\beta4$ or $Na_v\beta1.1$–$Na_v\beta1.4$) have thus far been identified (Catterall, 2000; Goldin, 2001; Catterall et al., 2005).

BFNIS is caused by missense mutations of SCN2A (Heron et al., 2002; Berkovic et al., 2004), the gene encoding $Na_v1.2$ Na^+ channel α subunit (see Fig. 1). It is an autosomal dominant disorder with high penetrance, characterized by afebrile seizures with onset before 4 months of age and spontaneous remission within the first year of life, without subsequent neurologic deficits. It is distinguished from benign familial neonatal seizures (BFNS) and from BFIS by an intermediate age at onset (Kaplan and Lacey, 1983). In particular, it is the first well characterized familial epilepsy syndrome in which all currently known mutations are in $Na_v1.2$. However, the identified mutations are not clustered in a specific region of the channel with known functional properties, and no functional studies have been done thus far. Therefore, there is no information about the pathogenic mechanism of BFNIS mutations.

It is important to investigate the functional effects of the mutations that cause BFNIS not only to clarify their epileptogenic mechanism but also to compare their effects with those of other Na^+ channel mutations that appear very similar but that cause much more severe phenotypes (Meisler and Kearney, 2005). The comparative study of the functional effects and the elucidation of the pathogenic mechanisms of epileptogenic mutations is essential for designing targeted and effective therapies for familial epilepsies. However, the functional analysis of Na^+ channel mutations has generated controversial results, because the functional properties of Na^+ channels are very sensitive to the cell back-

Received June 12, 2006; revised Aug. 10, 2006; accepted Aug. 13, 2006.

This study was supported in part by a grant from the Fondazione Pierfranco e Luisa Mariani. R.R. was the recipient of a fellowship from the Italian League Against Epilepsy. We thank Dr. William Catterall for sharing the $Na_v1.2$ clone and Giulia Giunti for help in some experiments.

Correspondence should be addressed to Dr. Massimo Mantegazza, Department of Neurophysiopathology, Istituto Neurologico Besta, Via Celoria 11, 20133 Milan, Italy. E-mail: mmantegazza@istituto-besta.it.

DOI:10.1523/JNEUROSCI.2476-06.2006

 0270-6474/06/2610100-10$15.00/0

ground and also the effects of pathogenic mutations are dependent on the expression system used (Baroudi et al., 2000; Chen et al., 2000; Cummins et al., 2001; Mantegazza et al., 2005b). To study BFNIS mutations with an experimental model that preserves neuronal properties and variety, we recorded Na^+ currents in transfected neocortical neurons maintained for short time periods in primary cultures. We report the functional study of four of the six identified BFNIS mutations (see Fig. 1). We show that the effects of the mutations are not homogeneous because they modify different properties of $Na_v1.2$, but the overall effect is consistent with neuronal hyperexcitability for all of them.

Materials and Methods

Mutagenesis. The mutations R223Q, R1319Q, L1563V, and L1330F were introduced in pCDM8–r$Na_v1.2a$ (encoding rat Na^+ channel $Na_v1.2a$ α subunit) by means of Quick Change XL Site Directed Mutagenesis kit (Stratagene, La Jolla, CA). The primers used were as follows: 5′GAACGTTCAGAGTTCTGCAGGCATTGAAAACAATATC forward and 5′GATATTGTTTTCAATGCCTGCAGAACTCTGAACGTTCTC reverse for R223Q; 5′CTACGAGCCTTATCCCAATTCGAAGGAATGAGGGTTG forward and 5′CAACCCTCATTCCTTCGAATTGGGATAAGGCTCGTAG reverse for R1319Q; 5′GACCAACATTGTGTACTGGATTAATCTGGTGTTCA forward and 5′TGAACACCAGATTAATCCAGTACACAATGTTGGTC reverse for L1563V; and 5′GGTTGTTGTAAACGCGTTCTTAGGCGCCATCC forward and 5′GGATGGCGCCTAAGAACGCGTTTACAACAACC reverse for L1330F. PCR product (2 μl), after *Dpn*I treatment, was used to transform TOP 10/P3 or MC1061/P3 chemically competent cells. The colonies were screened by digestion with a specific restriction enzyme because primers were designed to introduce also a silent restriction site. We confirmed the presence of the mutation of interest and the absence of spurious mutations by sequencing a portion of $Na_v1.2$ α subunit cDNA including the mutation site. Sequenced fragments with the desired mutation were then subcloned into the vector containing wild-type $Na_v1.2$ cDNA digesting both wild-type and mutant constructs with the same restriction enzymes (*Xba*I and *Xma*I for R223Q, *Bgl*II and *Bst*EII for R1319Q and L1330F, and *Bst*EII and *Xho*I for L1563V). We used this subcloning strategy to avoid the sequencing of the whole plasmid, which should be done to check for the presence of possible spurious mutations introduced by the PCR step.

Primary neuronal culture and transfections. Neocortical neurons were isolated from postnatal day 1 (P1) to P3 CD rat pups (Charles River, Civate, Italy). Rats were decapitated under ether anesthesia, and their brains were quickly removed and placed in ice-cold dissociation solution containing the following (in mM): 134 Na-isethionic acid, 23 glucose, 15 HEPES, 2 KCl, 4 $MgCl_2$, 0.1 $CaCl_2$, and 10 kynurenic acid, pH 7.4 with NaOH. Cerebral cortex was isolated using fine tweezers and chopped into small pieces that were then placed in a treatment chamber containing 1 mg/ml protease type XIV (Sigma, St. Louis, MO) in dissociation solution at 35°C. After 15 min of the enzyme treatment, the tissue was rinsed several times in dissociation solution and mechanically dissociated using a series of fire-polished Pasteur pipettes. The dissociated neurons were plated at a density of 1.5×10^6 cells per 35 mm Petri dish (Corning, Corning, NY). After allowing the neurons to settle for 1 h at 37°C, the dissociation solution was replaced with Neurobasal A culture medium (Invitrogen, Carlsbad, CA) supplemented with B27 (Invitrogen), 1 mM glutamine (Invitrogen), 10 ng/ml β-FGF (Invitrogen), 50 U/ml penicillin G (Sigma), and 50 μg/ml streptomycin (Sigma), and cultures were maintained at 37°C, 5%CO_2. The neurons were transfected on the same day with Lipofectamine 2000 (Invitrogen) and used within 30 h. The plasmid pEYFP–N1 (Clontech, Palo Alto, CA) expressing the enhanced yellow fluorescent protein was cotransfected with the construct of interest to select the transfected cells.

Electrophysiology. Transfected neurons were selected visually by their fluorescence using a Zeiss (Oberkochen, Germany) Axiovert 100 microscope equipped with a Chroma Technology (Rockingham, VT) 41028 epifluorescence excitation/emission cube.

Patch-clamp recordings were made at room temperature (23–25°C) using an Axopatch 1D amplifier, a Digidata 1322A acquisition board, and pClamp 8.2 software (Molecular Devices, Palo Alto, CA). Current signals were filtered at 10 kHz with the built-in four-pole low-pass Bessel filter and sampled at 100 kHz. The internal pipette solution contained the following (in mM): 110 NaCl, 35 tetraethylammonium-Cl, 1 $CaCl_2$, 2 $MgCl_2$, 0.3 $NiCl_2$, 0.4 $CdCl_2$, and 10 HEPES, pH 7.4 with NaOH. The bath solution contained the following (in mM): 140 K-gluconate, 5 EGTA, 10 HEPES, and 30 glucose, pH 7.4 with KOH. The bath solution was connected to the amplifier head-stage ground via an agar bridge containing 140 mM KCl. The recordings were corrected for junction potential errors by using the pClamp junction potential calculation system based on JPCalc software (P. H. Barry, University of New South Wales, Sydney, Australia). Capacitative currents were minimized by means of the amplifier circuitry. Series resistance compensation was not used because the maximum peak amplitude of Na^+ currents was <250 pA. The remaining transient and leakage currents were eliminated using P/4 subtraction. Patch pipettes were pulled from borosilicate glass tubing (Harvard Apparatus, Holliston, MA) with a P-97 Flaming-Brown horizontal puller (Sutter Instruments, Novato, CA) and heat polished directly before use. The diameter of the tip (~3 μm) and the shape of the pipettes were kept constant to maintain the area of the membrane patch approximately constant. Pipette resistance was in the range of 2.6–3.0 MΩ.

The current–voltage (*I–V*) relationships were obtained by applying depolarizing pulses from a −100 mV holding potential. The conductance–voltage (*g–V*) relationships (activation curves) were calculated from the *I–V* relationships according to $g = I_{Na}/(V - E_{Na})$, where I_{Na} is the peak Na^+ current measured at potential V, and E_{Na} is the current inversion potential experimentally measured applying depolarizing voltage steps (E_{Na} of 85 ± 4 mV; $n = 5$). The normalized activation and inactivation curves were fit to Boltzmann relationships in the following form: $y = 1/\{1 + \exp[(V - V_{1/2})/k]\}$, where y is normalized g_{Na} or I_{Na}, V is the membrane potential, $V_{1/2}$ is the voltage of half-maximal activation (V_a) or inactivation (V_h), and k is a slope factor. The inactivation protocol used a test pulse to −10 mV, preceded by 100-ms-long prepulses at depolarized potentials; holding potential was −100 mV. Inactivation kinetics were evaluated by fitting the current decay from the peak to a point 40 ms from the beginning of the voltage stimulus with an exponential relationship. Recovery from inactivation was studied with a test pulse to −10 mV, preceded by a 100-ms-long prepulse to −10 mV and by increasingly longer repolarizations to the holding potential (−100 mV). The recovery from inactivation data were fit to double exponentials.

Action potentials and subthreshold responses were recorded from layer V pyramidal neurons in rat neocortical slices as described previously (Mantegazza et al., 1998) and used as voltage stimuli in voltage-clamp experiments. They were sampled at 30 kHz to have a sufficiently high sampling frequency in the voltage-clamp recordings.

Data analysis. Fits were achieved using the Levenberg–Marquardt algorithm with Origin 7.5 (OriginLab, Northampton, MA). The fitting lines in the figures were obtained using mean parameters (shown in Tables 1, 2), calculated averaging the parameters of the fits of the single cells. The statistical analyses were made using Origin or Systat 9 (SPSS, Chicago, IL). The results are given as mean ± SEM, and threshold p value for statistical significance was 0.05. Statistical comparisons were performed with the *t* test or ANOVA with Tukey's *post hoc* test; homogeneity of variances was evaluated by means of the Brown–Forsythe test.

Results

Recording of Na^+ currents in transfected neocortical neurons in primary culture

To evaluate the properties of $Na_v1.2$ and of its epileptogenic mutants in neurons (Fig. 1), we transfected neocortical neurons in short-term primary cultures (30 h after plating) obtained from P1–P3 rats. The neocortex is a brain structure involved in the generation of epileptic seizures, thus appropriate for studying the effects of epileptogenic mutations. In addition, we assessed in preliminary experiments that these cultured neurons have relatively small Na^+ current.

The neurons in our cultures had heterogeneous morphologies, but two types were clearly distinguishable and consistently present: pyramidal-shaped cells and fusiform bipolar cells (supplemental Fig. 1, available at www.jneurosci.org as supplemental material). Neocortical pyramidal cells release glutamate and are the main class of excitatory projecting neurons, whereas fusiform cells are GABAergic interneurons that have usually inhibitory functions and are involved in local circuits (Cauli et al., 2000).

Cultured neurons develop processes that do not allow, using the whole-cell configuration of the patch-clamp technique, adequate voltage- and space-clamp control of the neuronal membrane required for the analysis of the gating of Na^+ channels. Thus, we used the on-cell macropatch configuration to record macroscopic Na^+ currents under good voltage- and space-clamp conditions and tested with this configuration whether our neuronal cultures were an appropriate experimental model for studying the properties of transfected Na^+ channels. In fact, exogenous subunits must be expressed at much higher levels than endogenous subunits to allow the selective study of their properties. In control experiments, we transfected the cultured neurons with a plasmid expressing yellow fluorescent protein (pEYFP–N1) to identify transfected cells by their fluorescence and to record the endogenous currents. We then cotransfected the cultures with the $Na_v1.2$-expressing plasmid pCDM8–$Na_v1.2$ and the plasmid pEYFP–N1 as reporter.

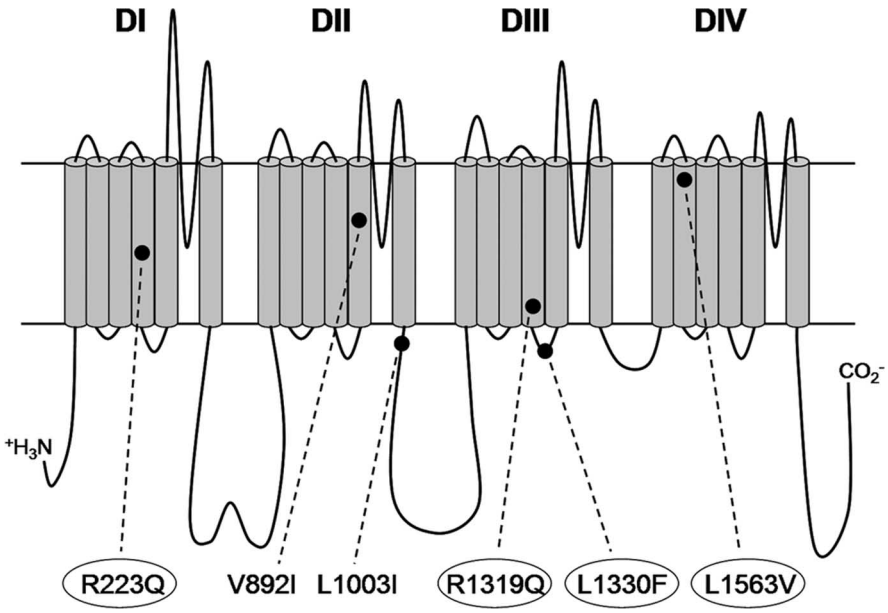

Figure 1. BNIFS mutations. The position of the six identified BNIFS mutations is indicated on the schematic membrane topology of the $Na_v1.2$ Na^+ channel α subunit. The mutation R1319Q has been identified in three different families. The mutations studied in this paper are highlighted by the ovals.

Figure 2 shows representative macropatch Na^+ currents recorded in transfected bipolar (Fig. 2*A*) and pyramidal (Fig. 2*B*) neurons. The top traces were recorded from neurons transfected with just pEYFP–N1, and the bottom traces were recorded from neurons cotransfected with pCDM8–$Na_v1.2$ and pEYFP–N1. The recordings showed a large increase in Na^+ current amplitude during transfection with the $Na_v1.2$-expressing plasmid. Figure 2, *C* and *D*, shows mean current–voltage plots obtained in bipolar and pyramidal neurons, respectively, applying test pulses to membrane potentials between −60 and +30 mV. The amplitude of the inward Na^+ current was maximal at approximately −15 mV in the bipolar neurons and −10 mV in the pyramidal neurons in control conditions and at approximately −5 mV in both bipolar and pyramidal neurons transfected with $Na_v1.2$. The transfection with $Na_v1.2$ induced on average a 12-fold increase in the maximum amplitude of the Na^+ current in bipolar neurons (from -12.6 ± 2.5 pA, $n = 20$, to -148 ± 17 pA, $n = 20$) and a ninefold increase in pyramidal neurons (from -18.6 ± 5.1 pA, $n = 10$, to -177 ± 25 pA, $n = 22$), thus indicating that the Na^+ current recorded in $Na_v1.2$-transfected neurons was mainly generated by the exogenous subunit. There was no significant difference in current amplitude between bipolar and pyramidal neurons.

Macropatch recordings permit accurate measurement of the properties of the Na^+ current, but the amplitude of the current in this configuration could be affected by clustering of channels in specialized plasma–membrane regions and by experimental factors that determine the area of the patch of membrane (e.g., the diameter of the tip of the pipette, the shape of the pipette, the amount of suction, etc.). We obtained reproducible results patching always the center of the soma, controlling the diameter and the shape of the pipette before each experiment, and applying gentle suction.

Thus, neocortical bipolar and pyramidal cultured neurons are a good experimental model for studying transfected Na^+ channels.

Properties of $Na_v1.2$ in transfected bipolar and pyramidal neocortical neurons

We studied the properties of $Na_v1.2$ in both bipolar and pyramidal neurons to find out whether they were cell type specific. Figure 3*A* shows average macropatch Na^+ currents recorded with a depolarizing step to −20 mV in bipolar and pyramidal neurons transfected with $Na_v1.2$. The time course of activation was similar in the two neuron subtypes as confirmed by the plot of the time to half-activation at a range of potentials, shown in the top of Figure 3*B*. The time course of the current decay was also similar in the two subtypes; it was well fit by a single-exponential relationship and was not significantly different at any potentials, as shown by the plot of the time constants of the fit of the decay at the indicated potentials (Fig. 3*B*, bottom). We quantified the persistent component of the Na^+ current (I_{NaP}) as the average current between 40 and 50 ms after the beginning of the depolarizing test pulse (Mantegazza et al., 2005b). I_{NaP} was at the limit of the experimental resolution at all of the potentials (<0.5% of the transient Na^+ current) and not significantly different between the two neuron subtypes (data not shown).

The voltage dependence of activation (Fig. 3*C*) was well fit by a single Boltzmann relationship and was not significantly different between bipolar and pyramidal neurons, with a half-activation potential of approximately −29 mV and a slope factor of 7.8 mV in bipolar neurons and of −28 mV and 7.6 mV in pyramidal neurons (Table 1). We measured the voltage dependence of inactivation (Fig. 3*C*) with a classical two-pulse protocol (100 ms inactivating pulses at the indicated potentials, followed by a test pulse at −10 mV); the data were well fit by a single

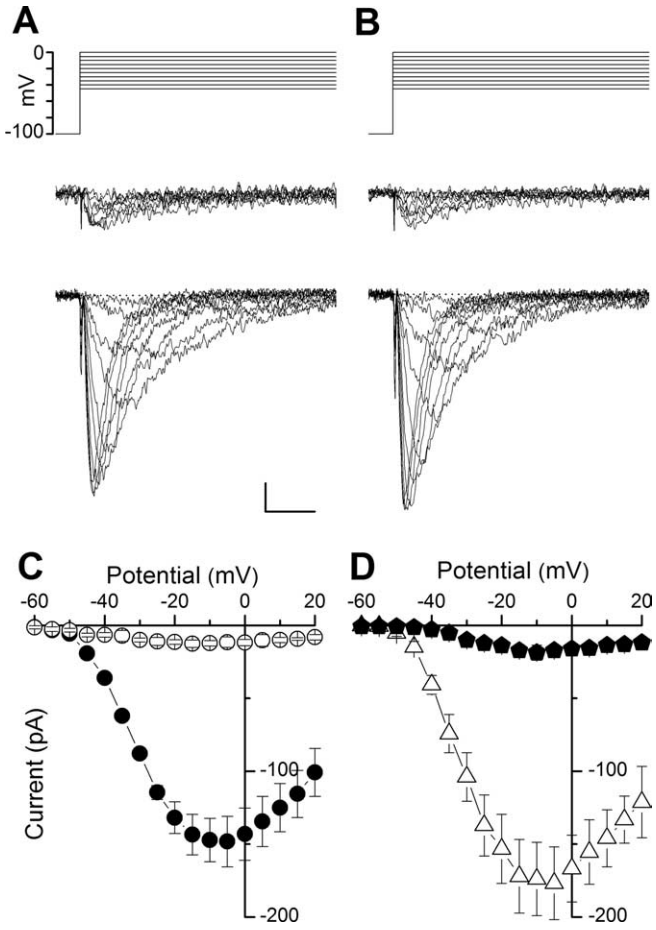

Figure 2. Macropatch Na^+ currents recorded in neurons transfected with $Na_v1.2$ Na^+ channel α subunit. ***A***, Middle, Macropatch Na^+ currents elicited by the voltage stimuli shown above in a representative control bipolar neuron transfected with YFP; bottom, macropatch Na^+ currents recorded applying the same voltage stimuli in a representative bipolar neuron transfected with $Na_v1.2$ Na^+ channel. Calibration: 50 pA, 1 ms. ***B***, Middle, Macropatch Na^+ currents recorded in a representative control pyramidal neuron transfected with YFP and elicited by the voltage stimuli shown above; bottom, macropatch Na^+ currents recorded in a representative pyramidal neuron transfected with $Na_v1.2$ and elicited by the voltage stimuli shown in the top. ***C***, Mean macropatch current–voltage curves for control YFP-transfected bipolar neurons (open circles) and bipolar neurons transfected with $Na_v1.2$ (filled circles). ***D***, Mean macropatch current–voltage curves for control YFP-transfected pyramidal neurons (filled pentagons) and pyramidal neurons transfected with $Na_v1.2$ (open triangles).

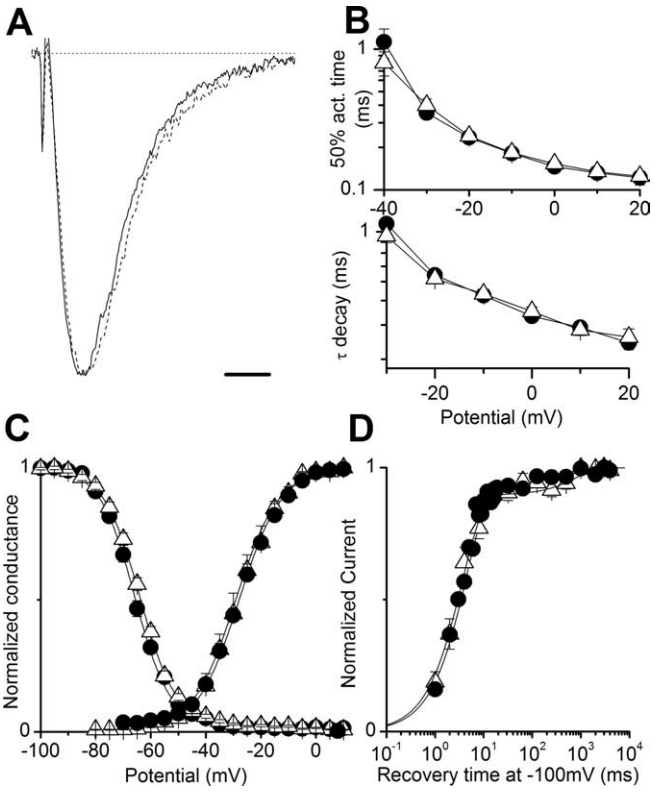

Figure 3. Properties of $Na_v1.2$ Na^+ currents in transfected neurons. ***A***, Average normalized macropatch current traces elicited with a depolarizing step to −20 mV for $Na_v1.2$-transfected pyramidal (solid line) and bipolar (dashed line) neurons. Horizontal calibration bar, 500 μs. ***B***, Top, Semilogarithmic plot of the time to half-activation at the indicated potentials for pyramidal (open triangles) and bipolar (filled circles) neurons; bottom, time constant of inactivation derived from fits of exponential functions to the decay of the current traces during depolarizations to the indicated potentials. ***C***, Mean voltage dependence of activation and inactivation; the lines are Boltzmann relationships whose parameters were calculated averaging the parameters of the fits of the single cells (Table 1). ***D***, Mean kinetics of recovery from a 100 ms inactivating pulse at −10 mV; the lines are double-exponential functions (Table 1).

Boltzmann relationship and not significantly different in the two neuron subtypes, with a half-inactivation potential of approximately −66 mV in bipolar neurons and −64 mV in pyramidal neurons, and a slope factor of 6.4 and 6.6 mV, respectively (Table 1). The kinetics of recovery from inactivation (Fig. 3*D*) was studied with an inactivating pulse of 100 ms at −10 mV, followed by a recovery period at −100 mV of increasing duration and by a test pulse at −10 mV. The data were well fit by the sum of two exponential functions, likely corresponding to recovery from fast and slow inactivation, and were not significantly different between the two neuron subtypes: the faster component had a time constant of ~4 ms and accounted for ~90% of the recovery, and the slower component was poorly resolved and had a time constant of ~1 s (Table 1).

Thus, $Na_v1.2$ has similar properties in transfected bipolar and pyramidal neocortical neurons. The four BFNIS mutants that we studied also had similar properties in the two neuronal subtypes (supplemental data, available at www.jneurosci.org as supplemental material). Therefore, we performed the statistical analysis using pooled data (Table 1).

Functional study of the mutation L1330F

The mutation L1330F was found in a BFNIS family with seven affected members over four generations (Heron et al., 2002). Seizures were often focal with secondary generalization, with head and eye deviation and sometimes lower limb jerks.

The mutation L1330F replaces a conserved leucine with a phenylalanine in the cytoplasmic linker between transmembrane segments S4 and S5 in domain III (DIII/S4–S5 loop) (Fig. 1). This cytoplasmic loop has been proposed to form part of the receptor for the channel inactivation gate, which is formed by the intracellular linker between domains III and IV (Catterall, 2000). Thus, it has been hypothesized that the mutation could reduce the rate of current decay and thus increase Na^+ currents causing hyperexcitability (Heron et al., 2002).

Figure 4 displays the analysis of macropatch recordings of $Na_v1.2$–L1330F transfected neurons compared with the pooled data obtained with wild-type $Na_v1.2$. Figure 4*A* shows average macropatch Na^+ currents recorded with a depolarizing step to −20 mV. The mutation did not have any significant effects on the kinetics of activation or inactivation, quantified in Figure 4*B*, top and bottom, respectively, which were similar to the control. The persistent component of the current was not significantly differ-

Table 1. Properties of wild-type and mutant $Na_v1.2$ currents elicited with voltage steps

	$Na_v1.2$ bipolar	$Na_v1.2$ pyramidal	$Na_v1.2$ pooled	L1330F pooled	L1563V pooled	R223Q pooled	R1319Q pooled
I_{MAX} (pA)	−148 ± 17 ($n = 20$)	−177 ± 25 ($n = 22$)	−157 ± 15 ($n = 42$)	−162 ± 16 ($n = 20$)	−132 ± 13 ($n = 19$)	−150 ± 17 ($n = 30$)	−151 ± 16 ($n = 19$)
V_a (mV)	−29.1 ± 0.8 ($n = 20$)	−28.0 ± 0.6 ($n = 22$)	−28.5 ± 0.5 ($n = 42$)	−27.9 ± 1.0 ($n = 20$)	**−33.6 ± 1.2 ($n = 19$) $p = 2 \times 10^{-5}$**	**−24.5 ± 0.6 ($n = 30$) $p = 4 \times 10^{-4}$**	**−25.9 ± 0.4 ($n = 19$) $p = 0.003$**
K_a (mV)	7.8 ± 0.2	7.6 ± 0.2	7.7 ± 0.1	7.1 ± 0.2	**6.2 ± 0.1 $p = 10^{-6}$**	8.1 ± 0.3	7.9 ± 0.2
V_h (mV)	−65.8 ± 0.7 ($n = 22$)	−64.0 ± 0.6 ($n = 26$)	−64.8 ± 0.5 ($n = 48$)	**−59.7 ± 0.7 ($n = 20$) $p = 2 \times 10^{-6}$**	−66.4 ± 0.8 ($n = 20$)	**−61.3 ± 0.5 ($n = 28$) $p = 1 \times 10^{-4}$**	**−61.0 ± 0.4 ($n = 18$) $p = 0.002$**
K_h (mV)	6.4 ± 0.2	6.6 ± 0.3	6.5 ± 0.2	**5.8 ± 0.2 $p = 0.01$**	6.3 ± 0.2	6.9 ± 0.3	6.2 ± 0.3
τ_1 (ms)	4.5 ± 0.6 ($n = 11$)	3.6 ± 0.9 ($n = 7$)	4.2 ± 0.5 ($n = 18$)	3.5 ± 0.9 ($n = 20$)	3.9 ± 0.5 ($n = 12$)	3.4 ± 0.6 ($n = 13$)	4.0 ± 0.4 ($n = 18$)
A_1	0.93 ± 0.04	0.89 ± 0.05	0.92 ± 0.03	0.90 ± 0.05	0.94 ± 0.07	0.90 ± 0.06	0.91 ± 0.06
τ_2 (ms)	1314 ± 496	890 ± 392	1037 ± 326	650 ± 420	1191 ± 456	787 ± 470	697 ± 427
A_2	0.07 ± 0.03	0.11 ± 0.04	0.08 ± 0.03	0.10 ± 0.04	0.06 ± 0.05	0.10 ± 0.04	0.09 ± 0.03

The properties of wild-type and mutant $Na_v1.2$ currents recorded in transfected neurons are shown. The parameters of the wild-type currents are shown for bipolar neurons, for pyramidal neurons, and for the pooled data. The parameters of the mutants are shown just for the pooled data (there was no significant difference between bipolar and pyramidal neurons, but see supplemental material, available at www.jneurosci.org as supplemental material). Statistically significant results are shown in bold, and the p value is indicated. I_{MAX}, Maximum current amplitude; V_a, voltage of half-maximal activation; K_a, slope factor of the activation curve; V_h, voltage of half-maximal inactivation; K_h, slope factor of the inactivation curve; τ_1, time constant of the first exponential of the fit of the recovery from inactivation; A_1, amplitude of the first exponential of the fit of the recovery from inactivation; τ_2, time constant of the second exponential of the fit of the recovery from inactivation; A_2, amplitude of the second exponential of the fit of the recovery from inactivation

ent. The amplitude of the macropatch current was also similar to wild-type $Na_v1.2$, as displayed by the *I–V* curve (Fig. 4*C*), suggesting that the mutation does not interfere with the plasma membrane targeting or the conductive properties of the channel. There were no significant changes in the voltage dependence of activation (Fig. 4*D*). However, the voltage dependence of inactivation (Fig. 4*E*) was significantly rightward shifted by ~5 mV compared with the wild type, and the slope factor was also significantly reduced (Table 1). Recovery from inactivation was unaffected by the mutation (Fig. 4*F*, Table 1).

Therefore, the voltage dependence of inactivation was the only functional parameter in which we observed an effect of the mutation. This finding is consistent with data obtained with glutamine scanning mutagenesis, which also suggested that this residue is critical for the voltage dependence of steady-state inactivation (Smith and Goldin, 1997).

This effect on Na^+ channel function may increase neuronal excitability because, at the typical resting potential of neocortical neurons (approximately −65 mV), ~30% of Na_v12–L1330F current is inactivated compared with ~50% of wild-type Na_v12 current, resulting in increased Na^+ current.

Functional study of the mutation L1563V

The mutation was identified in a BFNIS family with six affected members over four generations presenting with generalized or secondarily generalized seizures, often consisting of stiffening and jerking of the limbs (Lewis et al., 1996; Heron et al., 2002).

It replaces a conserved leucine with a valine in the second transmembrane segment of DIV (Fig. 1). There are few studies about the functional role of amino acids in DIV/S2 of Na^+ channels. According to functional and structural data mainly obtained studying K^+ channels, S2 segments are amphipathic α-helices containing conserved acidic residues and interfacing directly with lipids and proteins on opposite faces, in particular with the basic residues of transmembrane segment S4 (Papazian et al., 1995; Planells-Cases et al., 1995). In the crystal structure of the *shaker* Kv1.2 K^+ channel, S1 and S2 helices partially shield the arginine-containing S4 helix from the membrane lipids, forming electrostatic interactions with its basic residues (Long et al., 2005). In domain II of Na^+ channels, acidic residues of S2 and S3 segments can form electrostatic interactions with basic residues of S4, and their mutations alter Na^+ channel gating (Mantegazza and Cestele, 2005).

Figure 5 displays the analysis of the macropatch currents recorded in $Na_v1.2$–L1563V-transfected neurons compared with the results obtained with wild-type $Na_v1.2$. The average $Na_v1.2$–L1563V current elicited by a depolarizing step to −20 mV showed a slightly faster time course of activation compared with the wild-type channel (Fig. 5*A*). This finding was confirmed by measuring the time to half-activation at a range of potentials (Fig. 5*B*). In fact, at potentials more negative than −20 mV, the time of half-activation was significantly smaller for $Na_v1.2$–L1563V, whereas with stronger depolarizations mutant and wild-type channels converged toward a similar value. The time course of current decay was not significantly different (Fig. 5*B*, bottom). The persistent current was not increased. The amplitude of maximum $Na_v1.2$–L1563V current was also not significantly different compared with the wild-type channel (Fig. 5*C*, Table 1), but the current reached the peak at more negative potentials (approximately −20 mV compared with approximately −15 mV for the wild type). This finding was confirmed by analysis of the activation curve that was shifted approximately −5 mV and significantly steeper (Fig. 5*D*, Table 1). The voltage dependence of inactivation (Fig. 5*E*) and the recovery from inactivation (Fig. 5*F*) were not modified (Table 1).

Therefore, the mutation L1563V of domain IV enhances activation of $Na_v1.2$ channel causing a negative shift of the curve of voltage dependence of activation. The effect on the time course of activation is consistent with the shift in the voltage dependence and should not be a direct effect on the rate constants of the activation process. In fact, at very depolarized potentials, the time of half-activation did not show any difference (Fig. 5*B*, bottom). Experimental evidence points to a particularly important role of domain IV in the coupling between activation and fast inactivation (Bezanilla, 2000). However, our data are consistent with the observation that some mutations in DIV can selectively affect the voltage dependence of activation (Kontis et al., 1997; Sheets et al., 1999; Nguyen and Horn, 2002) and with the proposed coopera-

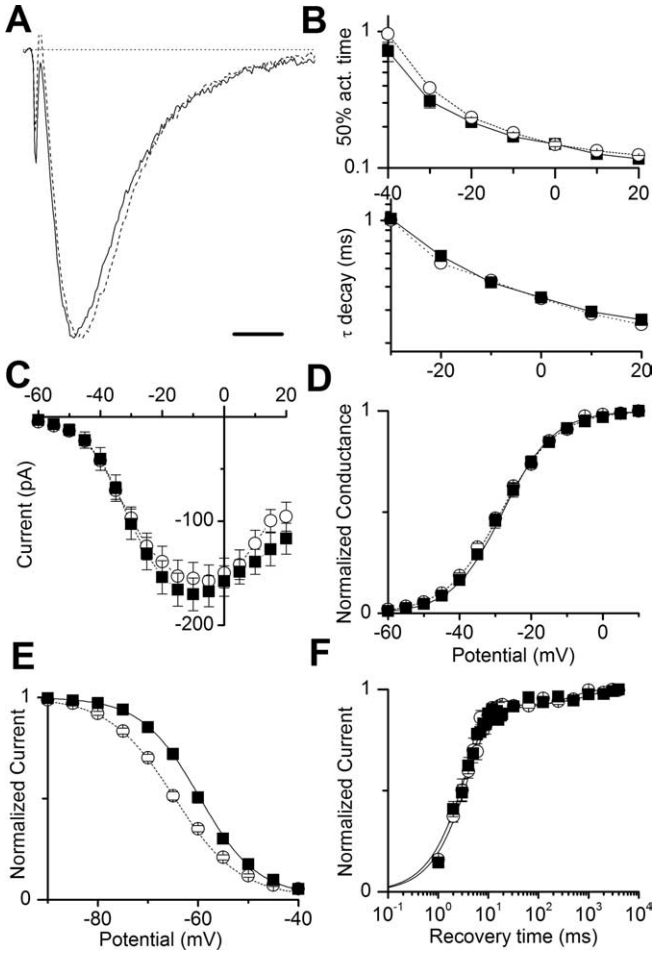

Figure 4. Functional effects of the mutation L1330F. ***A***, Average normalized macropatch current traces elicited with a depolarizing step to −20 mV in $Na_v1.2$–L1330F-transfected neurons (solid line, bipolar and pyramidal neurons pooled); average wild-type $Na_v1.2$ traces are shown for comparison (dashed line, bipolar and pyramidal neurons pooled). Horizontal calibration bar, 500 μs. ***B***, Top, Semilogarithmic plot of the time to half-activation at the indicated potentials for $Na_v1.2$–L1330F (squares) and wild-type $Na_v1.2$ (circles); bottom, time constant of inactivation derived from fits of exponential functions to the decay of the current traces during depolarizations to the indicated potentials. ***C***, Mean current–voltage plots. ***D***, Mean voltage dependence of activation; the lines are mean Boltzmann relationships (solid for L1330F; dashed for wild-type $Na_v1.2$) (Table 1). ***E***, Mean voltage dependence of inactivation; the lines are mean Boltzmann relationships (Table 1). ***F***, Mean kinetics of recovery from inactivation; the lines are mean fits of double-exponential functions to the data (Table 1).

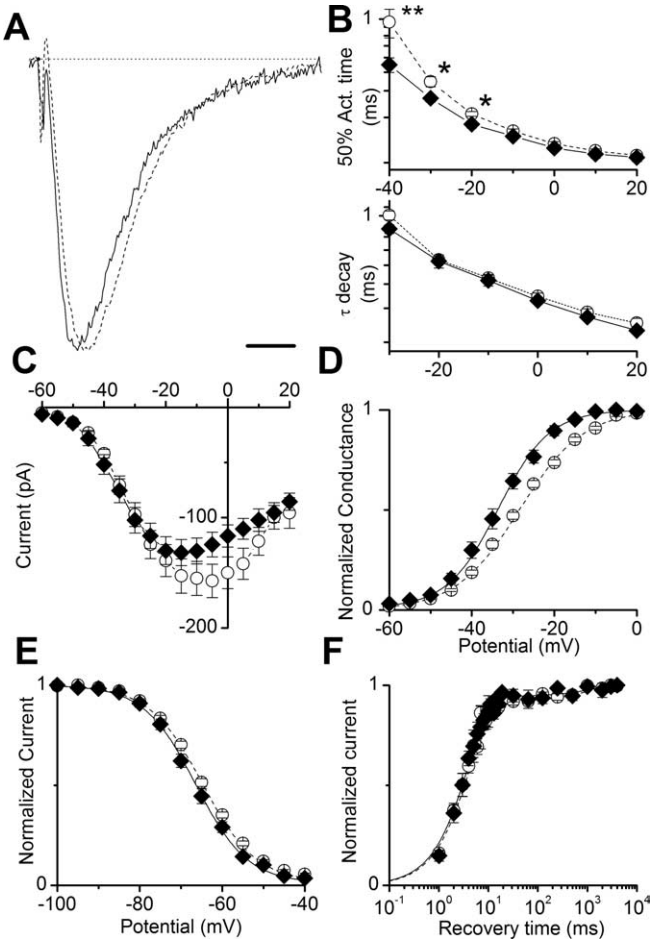

Figure 5. Functional effects of the mutation L1563V. ***A***, Average normalized macropatch current traces elicited with a depolarizing step to −20 mV in $Na_v1.2$–L1563V (solid line) and wild-type $Na_v1.2$ (dashed line) transfected neurons. Horizontal calibration bar, 500 μs. ***B***, Top, Semilogarithmic plot of the time to half-activation at the indicated potentials for $Na_v1.2$–L1563V (diamonds) and wild-type $Na_v1.2$ (circles). Statistically significant differences are indicated. Bottom, Time constant of inactivation derived from fits of exponential functions to the decay of the current traces during depolarizations to the indicated potentials. ***C***, Mean current–voltage plots. ***D***, Mean voltage dependence of activation; the lines are mean Boltzmann relationships (solid for L1563V; dashed for wild-type $Na_v1.2$) (Table 1). ***E***, Mean voltage dependence of inactivation; the lines are mean Boltzmann relationships (Table 1). ***F***, Mean kinetics of recovery from inactivation; the lines are mean fits of double-exponential functions to the data (Table 1). $*p \leq 0.05$; $**p \leq 0.01$.

tive interactions between domains in Na^+ channels (Chanda et al., 2004).

The negative shift of the activation curve is consistent with neuronal hyperexcitability, because mutant channels can be activated by weaker depolarizations than wild-type channels, resulting in increased Na^+ current.

Functional study of the mutations R233Q and R1319Q

The mutation R1319Q was found in three BFNIS families with a total of nine affected individuals and replaces a conserved arginine with a glutamine in the transmembrane segment S4 of domain III (Berkovic et al., 2004). Seizures in different individuals of the three families comprised clonic jerking of the eyelid and lower lip, tonic contraction of the four limbs, generalized rigidity and bilateral arm jerking, and head and eye deviation followed by bilateral limb jerking. The mutation R223Q replaces a conserved arginine with a glutamine in the transmembrane segment S4 of domain I. It has been identified in a BFNIS family with 17 affected individuals over four generations, but accurate characterization of the seizures was not possible (Berkovic et al., 2004). Both of the mutations neutralize voltage-sensing charges in S4 segments. Most studies suggest an outward rotational motion of the S4 or S4 and S3 to move voltage-sensing charges across the membrane electric field (Bezanilla, 2000; Catterall, 2000). The mutations R223Q and R1319Q neutralize the third positive charge of the S4 segment in DI and the sixth positive charge of the S4 segment in DIII, respectively. Mutations that replace the positive charges of the S4 segments with glutamine residues have been extensively used to study the role of the single charges in voltage sensing (Stuhmer et al., 1989; Chen et al., 1996; Kontis and Goldin, 1997; Kontis et al., 1997; Cestele et al., 2001). The reported effects were variable according to the residue neutralized, the channel isoform, and the expression system: both positive and negative shifts of the activation and inactivation curves were observed, with or without modifications of the slope. The mutation R223Q has

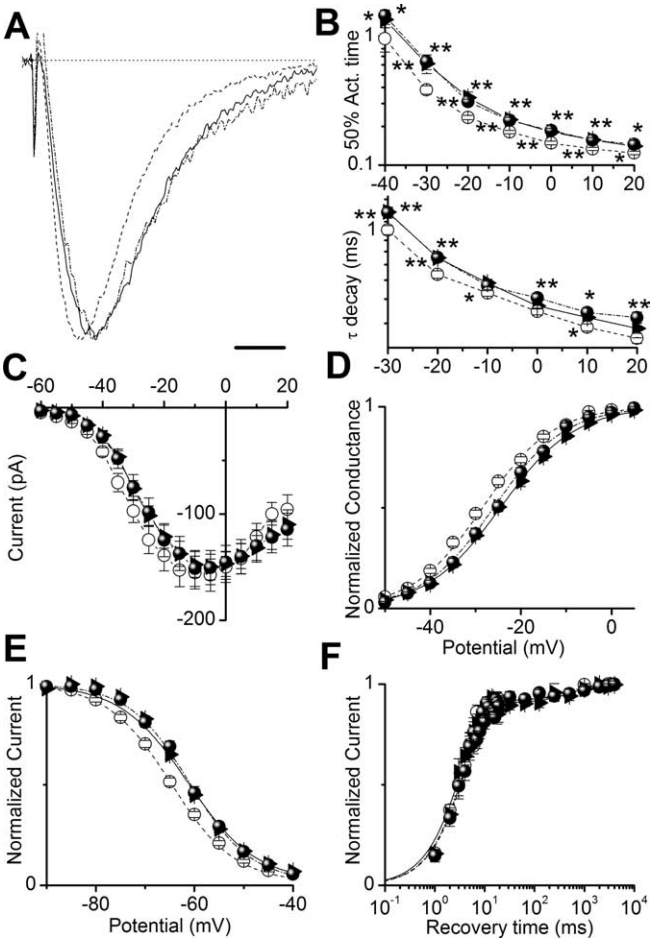

Figure 6. Functional effects of the mutations R223Q and R1319Q studied with classical voltage steps. ***A***, Average normalized macropatch current traces elicited with a depolarizing step to −20 mV in $Na_v1.2$–R223Q (solid line), $Na_v1.2$–R1319Q (dashed-dotted line), and wild-type $Na_v1.2$ (dashed line) transfected neurons. Horizontal calibration bar, 500 μs. ***B***, Top, Semilogarithmic plot of the time to half-activation at the indicated potentials for $Na_v1.2$–R223Q (triangles), $Na_v1.2$–R1319Q (spheres), and wild-type $Na_v1.2$ (circles); the statistical significance is indicated above the points for R1319Q and below the points for R223Q. Bottom, Time constant of inactivation derived from fits of exponential functions to the decay of the current traces during depolarizations to the indicated potentials. ***C***, Mean current–voltage plots. ***D***, Mean voltage dependence of activation; the lines are mean Boltzmann relationships (solid for R223Q, dashed-dotted for R1319Q, and dashed for wild-type $Na_v1.2$) (Table 1). ***E***, Mean voltage dependence of inactivation; the lines are mean Boltzmann relationships (Table 1). ***F***, Mean kinetics of recovery from inactivation; the lines are mean fits of double-exponential functions to the data (Table 1). $*p \leq 0.05$; $**p \leq 0.01$.

already been engineered in $Na_v1.2$ and studied in *Xenopus* oocytes, in which it caused barely significant positive shifts of the activation and inactivation curves (Stuhmer et al., 1989); the equivalent mutation in $Na_v1.5$ caused a positive shift of just the activation curve (Chen et al., 1996). The mutation R1319Q has never been studied before.

In our study, the functional effects of the mutations R223Q and R1319Q were similar and are shown and compared in Figure 6. The average currents showed a slower time course of activation and inactivation compared with wild-type $Na_v1.2$ (Fig. 6*A*). In fact, the mutant channels activated and inactivated more slowly than the wild type at all of the potentials tested (Fig. 6*B*). I_{NaP} was not significantly increased. The amplitude of the current was not affected by the mutations (Table 1), but the *I–V* plot shows a positive shift of the voltage dependence of the current (Fig. 6*C*). The curve of the voltage dependence of activation (Fig. 6*D*) confirms the shift observed in the *I–V* plot: the activation curve of R223Q shows a positive shift of ~4 mV, and the activation curve of R1319Q shows a positive shift of ~2.5 mV. The modifications of the slope of the activation curve did not reach statistical significance. The voltage dependence of inactivation was also modified (Fig. 6*E*, Table 1). In fact, the steady-state inactivation curve shows a positive shift of ~3.5 mV for R223Q and of ~3.8 mV for R1319Q. The recovery from inactivation was unaffected (Fig. 6*F*, Table 1).

Therefore, the two BFNIS mutations that target the voltage sensors have similar effects, modifying the voltage dependence of activation and inactivation. The modifications of the time course of activation and inactivation reflect in part the shift in the voltage dependence, as discussed for L1563V. However, the mutations R223Q and R1319Q could affect directly also the rate constants of the activation process and of the inactivation from the open state, because the kinetics are significantly different even at quite depolarized potentials at which the steady-state voltage-dependent properties should be similar.

The effects of these two mutations are statistically significant but quite small. This finding raises the concern of whether they can really affect neuronal functions. Moreover, some of the effects are consistent with decreased excitability (positive shift of the activation curve, slower activation kinetics) others with increased excitability (positive shift of the inactivation curve, slower inactivation kinetics). Thus, even if the modifications of Na^+ channel properties that we observed can actually perturb neuronal excitability, it is not clear in which direction.

To clarify this point, we studied the effects of R233Q and R1319Q applying physiological voltage stimuli: we recorded macropatch Na^+ currents using as command voltage subthreshold responses and action potentials, which we recorded from layer V pyramidal neurons in neocortical slices. The Na^+ currents elicited by these stimuli are those underling physiological membrane depolarizations. Thus, this method can better highlight the overall effect of the mutations, reproducing the physiological dynamic conditions of a firing neuron.

Figure 7*A* shows a subthreshold membrane response and an action potential recorded in current-clamp configuration in a layer V regular spiking neuron as described previously (Mantegazza et al., 1998), injecting the short depolarizing current stimuli that are shown in the bottom. Figure 7*B* displays the average currents elicited by the application of the subthreshold response as voltage stimulus, in neurons transfected with $Na_v1.2$, $Na_v1.2$–R223Q, and $Na_v1.2$–R1319Q. The resolution was improved by averaging the currents over multiple stimulations. The current elicited by the physiological stimulus was normalized for each cell to the peak value of the *I–V* plot obtained from the cell. The subthreshold current traces recorded in the neurons transfected with $Na_v1.2$–R223Q and $Na_v1.2$–R1319Q were larger than the wild-type current, and their peak values were significantly different compared with $Na_v1.2$ (Table 2). However, to have a measurement more representative of the whole time course of the current, we also integrated the normalized traces and compared their area. The bar graph in Figure 7*B* shows the area subtended by wild-type and mutant normalized currents; R223Q and R1319Q subthreshold currents resulted significantly larger than $Na_v1.2$ also with this comparison (Table 2).

Figure 7*C* compares the currents elicited applying as voltage stimulus the action potential. Normalized action currents were larger in neurons transfected with the mutant channels. In fact, both the peak amplitude of the current and the area

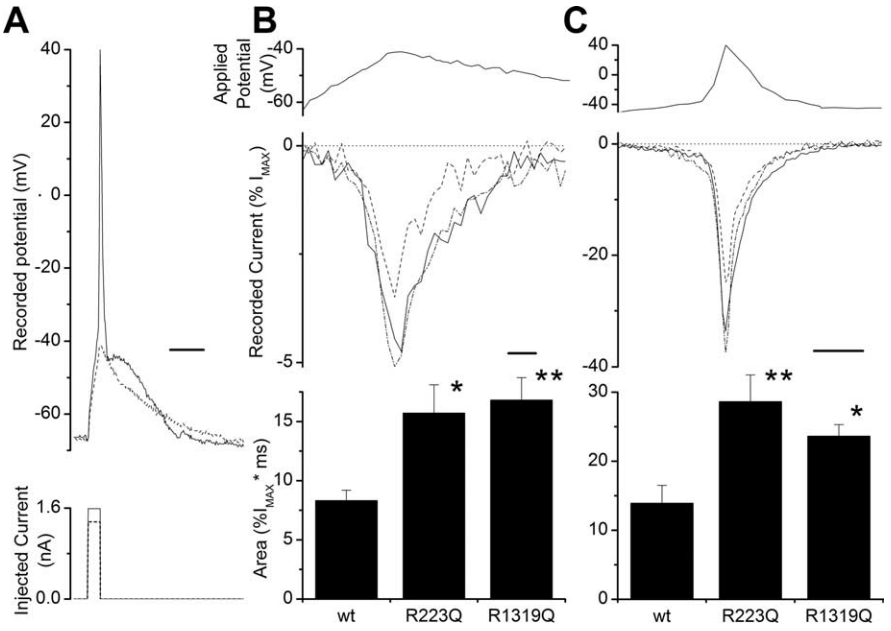

Figure 7. Functional effects of the mutations R223Q and R1319Q studied with physiological voltage stimuli. ***A***, Action potential and subthreshold response recorded with sharp microelectrodes in a layer V neuron in neocortical slices. The bottom is the injected depolarizing current pulse. Horizontal calibration bar, 10 ms. ***B***, Currents elicited in transfected neurons by the subthreshold response shown in ***A***. The top shows the subthreshold response used as voltage stimulus; the middle panel shows the recorded subthreshold currents (solid line for R223Q, dashed-dotted line for R1319Q, and dashed line for wild-type $Na_v1.2$). Horizontal calibration bar, 1 ms. The bar graph in the bottom shows the comparison between the area subtended by the subthreshold currents (Table 2). ***C***, Currents elicited in transfected neurons by the action potential shown in ***A***. The top shows the action potential used as voltage stimulus; the middle shows the recorded action currents (solid line for R223Q, dashed-dotted line for R1319Q, and dashed line for wild-type $Na_v1.2$). Horizontal calibration bar, 1 ms. The bar graph in the bottom shows the comparison between the area subtended by the action currents recorded in the three conditions (Table 2). wt, Wild type. $*p < 0.05$; $**p < 0.01$.

Table 2. Properties of wild-type and mutant $Na_v1.2$ currents elicited with physiological voltage stimuli

	$Na_v1.2$	R223Q	R1319Q
Subthreshold current peak (% I_{MAX})	3.5 ± 0.3 ($n = 19$)	**4.8 ± 0.4** ($n = 14$) **$p = 0.04$**	**5.1 ± 0.3** ($n = 14$) **$p = 0.03$**
Action current peak (% I_{MAX})	24.1 ± 4.0 ($n = 19$)	**33.6 ± 3.9** ($n = 15$) **$p = 0.03$**	**37.4 ± 3.8** ($n = 15$) **$p = 0.02$**
Subthreshold current area (% I_{MAX} × ms)	8.3 ± 0.9	**15.7 ± 2.4** **$p = 0.02$**	**16.8 ± 1.9** **$p = 0.004$**
Action current area (% I_{MAX} × ms)	15.1 ± 2.6	**28.6 ± 3.9** **$p = 0.009$**	**23.6 ± 1.7** **$p = 0.03$**

The table shows the properties of the Na^+ currents elicited using as voltage stimuli subthreshold responses and action potentials recorded in neocortical slices. The data are pooled for bipolar and pyramidal neurons. Statistically significant results are shown in bold, and the *p* value is indicated.

subtended by the current traces were significantly larger compared with wild-type $Na_v1.2$ (Table 2).

Thus, using physiological voltage-clamp stimuli, we were able to show that the overall functional effects of R223Q and R1319Q mutations are consistent with neuronal hyperexcitability, boosting depolarizations in the subthreshold range and better sustaining neuronal spikes.

Discussion

We investigated for the first time the functional effects of mutations of $Na_v1.2$ Na^+ channel that cause BFNIS (Fig. 1), which is an epileptic trait of the early infantile period characterized by afebrile secondarily generalized partial seizures with onset usually before 4 months of age and complete spontaneous remission within the first year of life. It is distinguished from BFNS, which begins at approximately the third day of life and is caused by mutations of KCNQ2 and KCNQ3 K^+ channel genes (Avanzini and Franceschetti, 2003), and it partially overlaps with BFIS, which typically begins at ~6 months of age and is very similar to BFNIS (Berkovic et al., 2004; Striano et al., 2006).

BFNIS is the only familial epileptic syndrome in which all known mutations are in $Na_v1.2$. In fact, excluding the missense mutation N1001K found in a family affected by BFIS (Striano et al., 2006), only two other mutations of $Na_v1.2$ have been identified in two Japanese families affected by other epilepsy syndromes. The missense mutation R188W has been identified in a patient with febrile seizures plus and complex partial epilepsy (Sugawara et al., 2001), but the penetrance was very low and other genes may be implicated (Ito et al., 2004). The truncation mutation R102X has been identified in a patient affected by an epilepsy similar to SMEI (Kamiya et al., 2004). However, SMEI and GEFS+ are mostly caused by mutations of $Na_v1.1$, and $Na_v1.2$ mutations appear thus far as exceptions (Meisler and Kearney, 2005).

The functional analysis of Na^+ channel epileptogenic mutations has provided a vast amount of data, but often the results have been controversial and dependent on the experimental system used (Meisler and Kearney, 2005). This variability can be at least in part attributable to the high sensitivity to the cell milieu of Na^+ channel properties (Baroudi et al., 2000; Chen et al., 2000; Cummins et al., 2001; Mantegazza et al., 2005b). We used transfected neocortical neurons in primary cultures because they provide an expression system that makes it possible to study exogenous channels while preserving neuronal properties, background, and variety. Neocortical neurons are particularly appropriate for studying BFNIS mutations because BFNIS is generated by cortical neuronal networks (Berkovic et al., 2004). Moreover, neurons prepared from immature animals are a good experimental model because BFNIS patients present with seizures only in the first year of life.

We studied wild-type and mutant channels in pyramidal and bipolar fusiform neurons, which correspond to typical excitatory and inhibitory cortical neurons, respectively (Cauli et al., 2000). The overall effect of all of the mutations that we studied is an increase of Na^+ current caused by modification of the gating properties of $Na_v1.2$ Na^+ channels, an effect that is consistent with neuronal hyperexcitability. The maximum current amplitude was not significantly different. In our experiments, this parameter could be affected by random errors attributable to the intrinsic limitations of the macropatch configuration (see Results) and by cell-to-cell variability in the expression level of the constructs. However, our results can rule out major differences in current amplitude among wild-type and mutant channels. Comparing the properties of the Na^+ current recorded in pyramidal and bipolar neurons, we observed only small differences in the properties of the wild-type channel and a trend toward a bigger

effect of the mutations in pyramidal neurons, but the differences did not reach the statistical significance (supplemental data, available at www.jneurosci.org as supplemental material). The effects that we observed are quite small, but this is consistent with the mild phenotype of the BFNIS patients, which present with just few clusters of seizures in the first year of life.

The homogeneous gain-of-function effect of the BFNIS mutations contrasts with the variability of the effects reported for other epileptogenic mutations of Na^+ channels. For instance, GEFS+ and SMEI mutations, which target mainly $Na_v1.1$ and $\beta1$ subunits, can cause both gain and loss of function (variability that could be at least in part attributable to the experimental models, see above), but a common effect is a complete loss of function (Meisler and Kearney, 2005). This may be consistent with different functional roles of $Na_v1.1$ and $Na_v1.2$ *in vivo*. For example, the two isoforms may differentially affect the excitability of excitatory and inhibitory neurons. In the cerebral cortex and in the hippocampus, $Na_v1.2$ is mainly localized in axons and nerve terminals and may be particularly highly expressed in excitatory pyramidal neurons, as suggested by the dense staining of excitatory fibers (Westenbroek et al., 1989; Gong et al., 1999; Whitaker et al., 2001) and by the selective clustering at nodes of Ranvier in developing myelinated fibers (Kaplan et al., 2001). Because of this distribution, the modifications of $Na_v1.2$ properties may preferentially affect the functions of excitatory neurons, causing network hyperexcitability. Interestingly, the distribution and developmental expression pattern of $Na_v1.2$ channels may also in part explain the spontaneous remission of BFNIS patients within the first year of life. In fact, $Na_v1.2$ channels are replaced by $Na_v1.6$ Na^+ channels in adult nodes of Ranvier (Kaplan et al., 2001); thus, BFNIS mutations may affect excitability of myelinated fibers during their development, but not at the stage of full nodal maturation. However, both network hyperexcitability and spontaneous remission may also in part be attributable to the development of GABAergic inhibition, which is mainly excitatory in early postnatal life (Cherubini et al., 1991).

In BFNIS patients, EEG recordings often show onset in the posterior areas (Heron et al., 2002; Berkovic et al., 2004). $Na_v1.2$ is expressed in all of the cortical areas studied (Westenbroek et al., 1989; Gong et al., 1999; Whitaker et al., 2001), but it could have higher expression in some regions, explaining the focal onset. However, posterior cortical areas can be a common region of generation of ictal and interictal EEG discharges in very young infants, for example, in severe epilepsies caused by extra-occipital brain lesions (Oka et al., 2004). These findings suggest that immature posterior cortical areas may be particularly susceptible to various types of neuronal hyperexcitability, including those resulting from $Na_v1.2$ dysfunctions. The widespread expression of $Na_v1.2$ in the CNS may favor the spreading of cortical excitability, leading to the generalized seizures often reported in BFNIS patients.

References

Avanzini G, Franceschetti S (2003) Cellular biology of epileptogenesis. Lancet Neurol 2:33–42.

Baroudi G, Carbonneau E, Pouliot V, Chahine M (2000) SCN5A mutation (T1620M) causing Brugada syndrome exhibits different phenotypes when expressed in Xenopus oocytes and mammalian cells. FEBS Lett 467:12–16.

Berkovic SF, Heron SE, Giordano L, Marini C, Guerrini R, Kaplan RE, Gambardella A, Steinlein OK, Grinton BE, Dean JT, Bordo L, Hodgson BL, Yamamoto T, Mulley JC, Zara F, Scheffer IE (2004) Benign familial neonatal-infantile seizures: characterization of a new sodium channelopathy. Ann Neurol 55:550–557.

Bezanilla F (2000) The voltage sensor in voltage-dependent ion channels. Physiol Rev 80:555–592.

Catterall WA (2000) From ionic currents to molecular mechanisms: the structure and function of voltage-gated sodium channels. Neuron 26:13–25.

Catterall WA, Goldin AL, Waxman SG (2005) International Union of Pharmacology. XLVII. Nomenclature and structure-function relationships of voltage-gated sodium channels. Pharmacol Rev 57:397–409.

Cauli B, Porter JT, Tsuzuki K, Lambolez B, Rossier J, Quenet B, Audinat E (2000) Classification of fusiform neocortical interneurons based on unsupervised clustering. Proc Natl Acad Sci USA 97:6144–6149.

Cestele S, Scheuer T, Mantegazza M, Rochat H, Catterall WA (2001) Neutralization of gating charges in domain II of the sodium channel alpha subunit enhances voltage-sensor trapping by a beta-scorpion toxin. J Gen Physiol 118:291–302.

Chanda B, Asamoah OK, Bezanilla F (2004) Coupling interactions between voltage sensors of the sodium channel as revealed by site-specific measurements. J Gen Physiol 123:217–230.

Chen LQ, Santarelli V, Horn R, Kallen RG (1996) A unique role for the S4 segment of domain 4 in the inactivation of sodium channels. J Gen Physiol 108:549–556.

Chen YH, Dale TJ, Romanos MA, Whitaker WR, Xie XM, Clare JJ (2000) Cloning, distribution and functional analysis of the type III sodium channel from human brain. Eur J Neurosci 12:4281–4289.

Cherubini E, Gaiarsa JL, Ben Ari Y (1991) GABA: an excitatory transmitter in early postnatal life. Trends Neurosci 14:515–519.

Cummins TR, Aglieco F, Renganathan M, Herzog RI, Dib-Hajj SD, Waxman SG (2001) Nav1.3 sodium channels: rapid repriming and slow closed-state inactivation display quantitative differences after expression in a mammalian cell line and in spinal sensory neurons. J Neurosci 21:5952–5961.

George Jr AL (2005) Inherited disorders of voltage-gated sodium channels. J Clin Invest 115:1990–1999.

Goldin AL (2001) Resurgence of sodium channel research. Annu Rev Physiol 63:871–894.

Gong B, Rhodes KJ, Bekele-Arcuri Z, Trimmer JS (1999) Type I and type II Na^+ channel alpha-subunit polypeptides exhibit distinct spatial and temporal patterning, and association with auxiliary subunits in rat brain. J Comp Neurol 412:342–352.

Heron SE, Crossland KM, Andermann E, Phillips HA, Hall AJ, Bleasel A, Shevell M, Mercho S, Seni MH, Guiot MC, Mulley JC, Berkovic SF, Scheffer IE (2002) Sodium-channel defects in benign familial neonatal-infantile seizures. Lancet 360:851–852.

Ito M, Shirasaka Y, Hirose S, Sugawara T, Yamakawa K (2004) Seizure phenotypes of a family with missense mutations in SCN2A. Pediatr Neurol 31:150–152.

Kamiya K, Kaneda M, Sugawara T, Mazaki E, Okamura N, Montal M, Makita N, Tanaka M, Fukushima K, Fujiwara T, Inoue Y, Yamakawa K (2004) A nonsense mutation of the sodium channel gene SCN2A in a patient with intractable epilepsy and mental decline. J Neurosci 24:2690–2698.

Kaplan MR, Cho MH, Ullian EM, Isom LL, Levinson SR, Barres BA (2001) Differential control of clustering of the sodium channels $Na_v1.2$ and $Na_v1.6$ at developing CNS nodes of Ranvier. Neuron 30:105–119.

Kaplan RE, Lacey DJ (1983) Benign familial neonatal-infantile seizures. Am J Med Genet 16:595–599.

Kontis KJ, Goldin AL (1997) Sodium channel inactivation is altered by substitution of voltage sensor positive charges. J Gen Physiol 110:403–413.

Kontis KJ, Rounaghi A, Goldin AL (1997) Sodium channel activation gating is affected by substitutions of voltage sensor positive charges in all four domains. J Gen Physiol 110:391–401.

Lewis TB, Shevell MI, Andermann E, Ryan SG, Leach RJ (1996) Evidence of a third locus for benign familial convulsions. J Child Neurol 11:211–214.

Long SB, Campbell EB, Mackinnon R (2005) Voltage sensor of Kv1.2: structural basis of electromechanical coupling. Science 309:903–908.

Mantegazza M, Cestele S (2005) Beta-scorpion toxin effects suggest electrostatic interactions in domain II of voltage-dependent sodium channels. J Physiol (Lond) 568:13–30.

Mantegazza M, Franceschetti S, Avanzini G (1998) Anemone toxin (ATX II)-induced increase in persistent sodium current: effects on the firing properties of rat neocortical pyramidal neurones. J Physiol (Lond) 507:105–116.

Mantegazza M, Gambardella A, Rusconi R, Schiavon E, Annesi F, Cassulini

RR, Labate A, Carrideo S, Chifari R, Canevini MP, Canger R, Franceschetti S, Annesi G, Wanke E, Quattrone A (2005a) Identification of an Nav1.1 sodium channel (SCN1A) loss-of-function mutation associated with familial simple febrile seizures. Proc Natl Acad Sci USA 102:18177–18182.

Mantegazza M, Yu FH, Powell AJ, Clare JJ, Catterall WA, Scheuer T (2005b) Molecular determinants for modulation of persistent sodium current by G-protein $\beta\gamma$ subunits. J Neurosci 25:3341–3349.

Meisler MH, Kearney JA (2005) Sodium channel mutations in epilepsy and other neurological disorders. J Clin Invest 115:2010–2017.

Nguyen TP, Horn R (2002) Movement and crevices around a sodium channel S3 segment. J Gen Physiol 120:419–436.

Noebels JL (2003) The biology of epilepsy genes. Annu Rev Neurosci 26:599–625.

Oka M, Kobayashi K, Akiyama T, Ogino T, Oka E (2004) A study of spike-density on EEG in West syndrome. Brain Dev 26:105–112.

Papazian DM, Shao XM, Seoh SA, Mock AF, Huang Y, Wainstock DH (1995) Electrostatic interactions of S4 voltage sensor in Shaker K^+ channel. Neuron 14:1293–1301.

Planells-Cases R, Ferrer-Montiel AV, Patten CD, Montal M (1995) Mutation of conserved negatively charged residues in the S2 and S3 transmembrane segments of a mammalian K^+ channel selectively modulates channel gating. Proc Natl Acad Sci USA 92:9422–9426.

Sheets MF, Kyle JW, Kallen RG, Hanck DA (1999) The Na channel voltage sensor associated with inactivation is localized to the external charged residues of domain IV, S4. Biophys J 77:747–757.

Smith MR, Goldin AL (1997) Interaction between the sodium channel inactivation linker and domain III S4–S5. Biophys J 73:1885–1895.

Striano P, Bordo L, Lispi ML, Specchio N, Minetti C, Vigevano F, Zara F (2006) A novel SCN2A mutation in family with benign familial infantile seizures. Epilepsia 47:218–220.

Stuhmer W, Conti F, Suzuki H, Wang XD, Noda M, Yahagi N, Kubo H, Numa S (1989) Structural parts involved in activation and inactivation of the sodium channel. Nature 339:597–603.

Sugawara T, Tsurubuchi Y, Agarwala KL, Ito M, Fukuma G, Mazaki-Miyazaki E, Nagafuji H, Noda M, Imoto K, Wada K, Mitsudome A, Kaneko S, Montal M, Nagata K, Hirose S, Yamakawa K (2001) A missense mutation of the Na^+ channel alpha II subunit gene $Na_v1.2$ in a patient with febrile and afebrile seizures causes channel dysfunction. Proc Natl Acad Sci USA 98:6384–6389.

Westenbroek RE, Merrick DK, Catterall WA (1989) Differential subcellular localization of the RI and RII Na^+ channel subtypes in central neurons. Neuron 3:695–704.

Whitaker WR, Faull RL, Waldvogel HJ, Plumpton CJ, Emson PC, Clare JJ (2001) Comparative distribution of voltage-gated sodium channel proteins in human brain. Brain Res Mol Brain Res 88:37–53.